Extreme wave runup on a vertical cliff

Francesco Carbone,[1] Denys Dutykh,[1,2] John M. Dudley,[3] and Frédéric Dias[1,4]

Received 24 May 2013; accepted 5 June 2013; published 25 June 2013.

[1] Wave impact and runup onto vertical obstacles are among the most important phenomena which must be taken into account in the design of coastal structures. From linear wave theory, we know that the wave amplitude on a vertical wall is twice the incident wave amplitude with weakly nonlinear theories bringing small corrections to this result. In this present study, however, we show that certain simple wave groups may produce much higher runups than previously predicted, with particular incident wave frequencies resulting in runup heights exceeding the initial wave amplitude by a factor of 5, suggesting that the notion of the design wave used in coastal structure design may need to be revisited. The results presented in this study can be considered as a note of caution for practitioners, on one side, and as a challenging novel material for theoreticians who work in the field of extreme wave-coastal structure interaction.
Citation: Carbone, F., D. Dutykh, J. M. Dudley, and F. Dias (2013), Extreme wave runup on a vertical cliff, *Geophys. Res. Lett.*, *40*, 3138–3143, doi:10.1002/grl.50637.

1. Introduction

[2] The robust design of various coastal structures (such as sea-walls and breakwaters) relies on the accurate estimation of the wave loading forces. To this end, engineers have introduced the notion of the so-called *design wave*. Once the particular characteristics of this design wave are determined, the pressure field inside the bulk of fluid is usually reconstructed (in the engineering practice) using the *Sainflou* [1928] or *Goda* [2010] semiempirical formulas. However, there is a difficulty in determining the wave height to be used in design works. Sometimes, it is taken as the significant wave height $H_{1/3}$, but in other cases, it is $H_{1/10}$ (the average of 10% highest waves) that is substituted into the wave pressure formulas. If we take, for example, an idealized sea state which consists only of a single monochromatic wave component with amplitude a_0, its wave height H_0 can be trivially computed

$$H_0 \equiv H_{1/3} \equiv H_{1/10} \equiv 2a_0. \tag{1}$$

Consequently, the design wave will have also the height equal to $2a_0$.

[3] In the present study, we show that even such simple monochromatic sea states, subject to the nonlinear dynamics over a constant bottom, can produce much higher amplitudes on a vertical wall. Namely, we show below that some wave frequencies can lead to an extreme runup of the order of $\approx 5.5a_0$ on the cliff. The results presented in this study suggest that the notion of the design wave has to be revisited. Moreover, the mechanism elucidated in this work can shed some light onto the freak wave phenomenon in the shallow water regime, where we recall in this context that over 80% of reported past freak wave events have been in shallow waters or coastal areas [*Nikolkina and Didenkulova*, 2011; *O'Brien et al.*, 2013].

[4] It is well known that wave propagation on the free surface of an incompressible homogeneous inviscid fluid is described by the Euler equations combined with nonlinear boundary conditions on the free surface [*Stoker*, 1957]. However, this problem is difficult to solve over large domains, and consequently, simplified models are often used. In particular, in this study, we focus our attention on long wave propagation. A complete description of wave processes, including collisions and reflections, is achieved by employing two-way propagation models of Boussinesq type [*Bona and Chen*, 1998]. Taking into account the fact that we are interested here in modeling (potentially) high amplitude waves, we adopt the fully nonlinear Serre-Green-Naghdi (SGN) equations [*Serre*, 1953; *Green et al.*, 1974; *Green and Naghdi*, 1976; *Zheleznyak and Pelinovsky*, 1985], which make no restriction on the wave amplitude. Only the weak dispersion assumption is adopted in the mathematical derivations of this model [*Wei et al.*, 1995; *Lannes and Bonneton*, 2009; *Dias and Milewski*, 2010].

[5] We consider a two-dimensional wave tank with a flat impermeable bottom of uniform depth $d = \text{const}$, filled with an incompressible, inviscid fluid (see Figure 1). The Cartesian coordinate system Oxy is chosen such that the y-axis points vertically upward and the horizontal x-axis coincides with the undisturbed water level $y = 0$. The free surface elevation with respect to the still water level is denoted by $y = \eta(x,t)$, and hence, the total water depth is given by $h(x,t) = d + \eta(x,t)$. Denoting the depth-averaged horizontal velocity by $u(x,t)$, the SGN system reads [*Lannes and Bonneton*, 2009; *Dias and Milewski*, 2010; *Clamond and Dutykh*, 2012]:

$$h_t + (hu)_x = 0, \tag{2}$$

$$u_t + \left(\frac{1}{2}u^2 + gh\right)_x = \frac{1}{3}h^{-1}\left[\, h^3\left(u_{xt} + uu_{xx} - u_x^2\right)\right]_x, \tag{3}$$

where g is the acceleration due to gravity.

[1]School of Mathematical Sciences, University College of Dublin, Dublin, Ireland.
[2]Université de Savoie-CNRS, Laboratoire de Mathématiques LAMA – UMR 5127, Le Bourget-du-Lac, France.
[3]Institut FEMTO-ST, UMR 6174 CNRS, Université de Franche-Comté, Besançon, France.
[4]CMLA, ENS Cachan, Cachan, France.

Corresponding author: F. Carbone, School of Mathematical Sciences, University College of Dublin, Dublin, Ireland. (francesco.carbone@ucd.ie)

0094-8276/13/10.1002/grl.50637

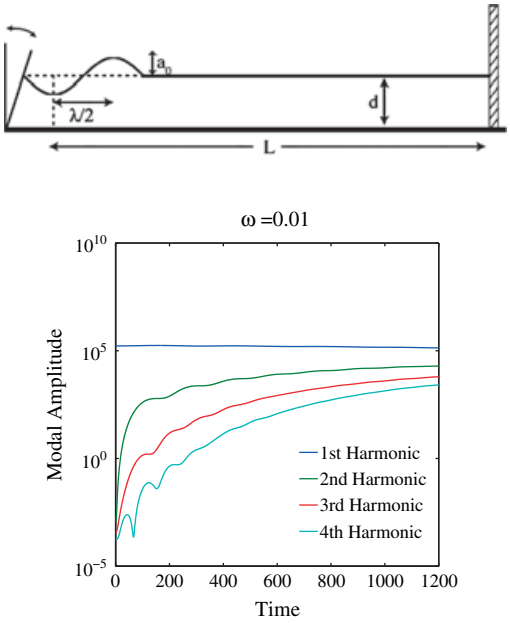

Figure 1. (top) Schematic view of the numerical experiments. Here L is the length of the computational domain, d is the uniform water depth, a_0 is the incoming wave amplitude, and λ is its wavelength. (bottom) Temporal evolution of the first four harmonics of a sinusoidal wave of frequency $\omega = 0.01$ injected in the domain (in the absence of the right wall).

[6] The SGN system possesses Hamiltonian and Lagrangian structures [*Li*, 2002; *Clamond and Dutykh*, 2012] and conservation laws for mass, momentum, potential vorticity, and energy [*Li*, 2002] (Dutykh et al. arXiv:1104.4456). From a more physical perspective, the SGN model combines strong nonlinear effects with some dispersion that approximates well the full water wave dynamics. This model has been previously validated by extensive comparisons with experimental data for wave propagation and runup [*Chazel et al.*, 2011; *Tissier et al.*, 2011; *Carter and Cienfuegos*, 2011] (Dutykh et al. arXiv:1104.4456).

[7] One of the most important questions in water wave theory is the understanding of wave interactions and reflections [*Linton and McIver*, 2001; *Berger and Milewski*, 2003; *Clamond et al.*, 2006] and the interaction of solitary waves has also been extensively studied [*Zabusky and Kruskal*, 1965; *Bona et al.*, 1980; *Fenton and Rienecker*, 1982; *Craig et al.*, 2006]. By using symmetry arguments, one can show that the head-on collision of two equal solitary waves is equivalent to the solitary wave/wall interaction in the absence of viscous effects.

[8] The accurate determination of the maximum wave height on a wall is of primary importance for applications. Several analytical predictions for periodic or solitary wave runup $R_{\max}$ in terms of the dimensionless wave amplitude $\alpha = a_0/d$ have been developed: linear theory [*Mei*, 1989] $R_{\max}/d = 2\alpha$, third-order theory [*Su and Mirie*, 1980] $R_{\max}/d = 2\alpha + 1/2\alpha^2 + 3/4\alpha^3$, and nonlinear shallow water theory [*Mirchina and Pelinovsky*, 1984] $R_{\max}/d = 4\left(1+\alpha-\sqrt{1+\alpha}\right) = 2\alpha + 1/2\alpha^2 - 1/4\alpha^3 + \mathcal{O}(\alpha^4)$.

[9] These results have been confirmed in previous experimental [*Maxworthy*, 1976], theoretical [*Byatt-Smith*, 1988], and numerical [*Fenton and Rienecker*, 1982; *Craig et al.*, 2006] studies. All these theories agree on the fact that the wave height on the wall is 2 times the incident wave amplitude plus higher order corrections. This conclusion provides a theoretical justification for the use of a wave height such as $H_{1/3}$ in the design wave definition.

2. Numerical Study

[10] From a practical point of view, however, the reasoning presented above contains at least one serious flaw—in real-world conditions, waves seldom come isolated but rather as groups. In this section, we show numerically how simple wave groups can produce much higher runups than expected from the existing theoretical predictions.

[11] Our numerical wave periods cover a range between 20 s and 1100 s (i.e., for $6 < d < 30$ m and $g = 9.81$ m/s^2), from long swells to tsunami waves. Extreme runups are obtained for wave periods which are in between swell periods and tsunamis periods, corresponding possibly to tsunamis generated by underwater landslides. Moreover, we take as initial conditions waves which are not exact solutions to the equations. Naturally, they deform as they evolve toward the vertical wall. This deformation is reminiscent of the transformation of waves over sloping bathymetries.

2.1. Numerical Scheme and Setup

[12] Let us consider a flat channel of constant depth d and length L. This channel is bounded on the right by a rigid vertical wall and by a wavemaker on the left (see Figure 1). We use dimensionless variables where lengths are normalized with d, speeds with $\sqrt{gd}$, and time with $\sqrt{d/g}$. This scaling is equivalent to setting $g = 1$ m/s^2, $d = 1$ m in the governing equations (2) and (3).

[13] In order to solve numerically the SGN equations, we use the high-order finite-volume scheme described in Dutykh et al. (arXiv:1104.4456). This scheme has been successfully validated against analytical solutions and experimental data [*Hammack et al.*, 2004]. For the time integration, we use the classical fourth-order Runge-Kutta scheme [*Shampine*, 1994; *Shampine and Reichelt*, 1997]. The computational domain is divided into equal intervals (i.e., control volumes) such that we have $N = 1000$ control volumes per wavelength. The convergence study showed that this grid provides a good trade-off between accuracy and overall computational time. Note that the extreme runup values reported in this study can slightly increase under mesh refinement, which decreases the effect of numerical dissipation. All simulations start with the rest state $\eta(x, t = 0) \equiv 0$, $u(x, t = 0) \equiv 0$. The wavemaker generates on the left boundary, during a time T, the following periodic free surface disturbance with corresponding fluid velocity:

$$\eta(x = 0, t) = \eta_0(t) = a_0 \sin(\omega t)\mathcal{H}(T - t), \tag{4}$$

$$u(x = 0, t) = \frac{\eta_0(t) c_s}{d + \eta_0(t)}, \tag{5}$$

where the amplitude $a_0 = 0.05$, $\omega \in [0.01, 0.25]$, $\mathcal{H}(t)$ is the Heaviside function, and c_s is the wave speed

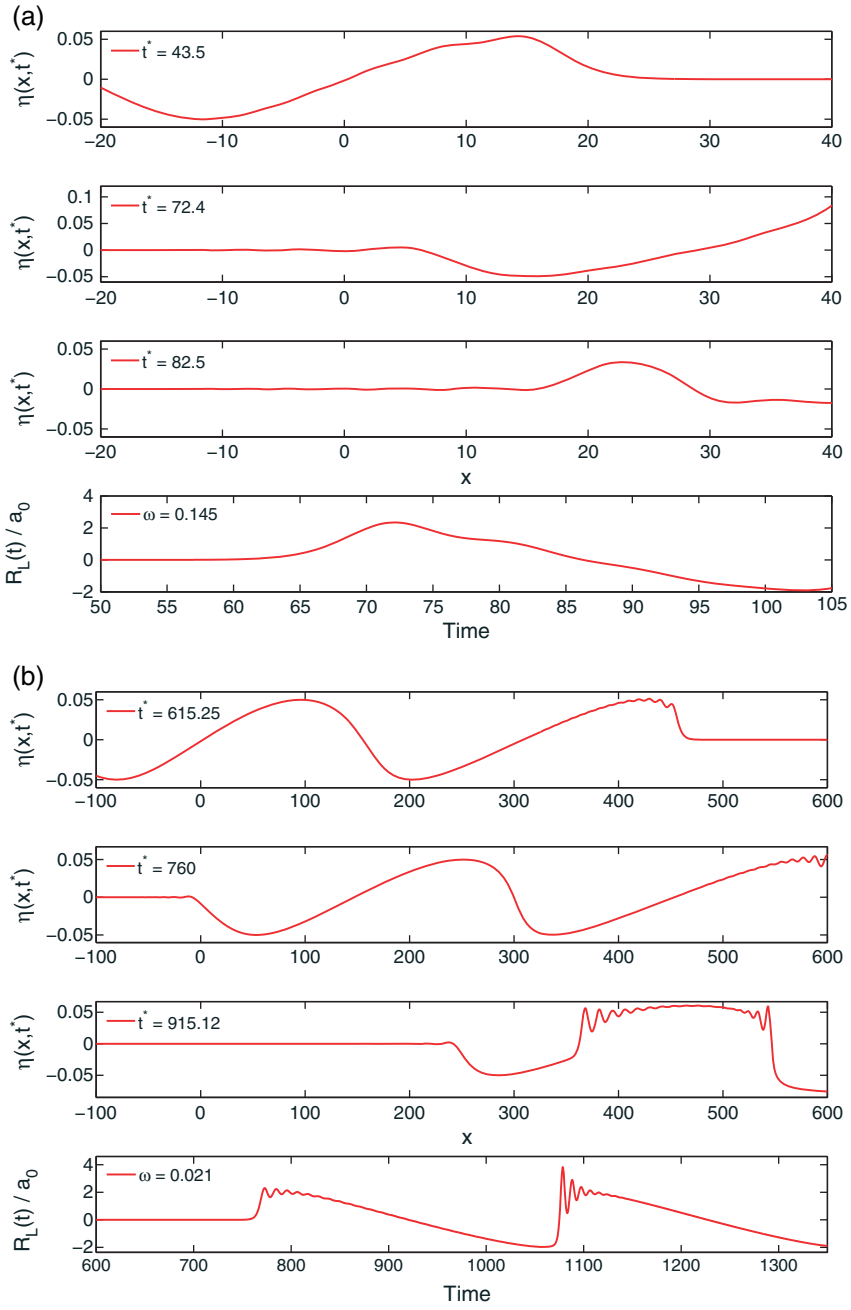

Figure 2. Time evolution of the free surface elevation as a function of space, at three different times t^* (first three top panels of Figures 2a–2c) reported on the figure. The bottom panel of Figure 2a refers to the single-wave case with frequency $\omega = 0.145$, the bottom panel of Figure 2b refers to the two-wave case with frequency $\omega = 0.021$, and the bottom panel of Figure 2c refers to the three-wave case with frequency $\omega = 0.0315$. The bottom panel of each column reports the maximal elevation at the wall R_L/a_0 as a function of time.

$c_s = \sqrt{g(d+a_0)}$ (Dutykh et al. arXiv:1104.4456). An important remark should be made on the initialization of the problem: sometimes spurious high-frequency standing waves are generated when numerical simulations of nonlinear progressive waves are initialized using linear waves (in particular, for deep water waves). In such cases, the problem should be initialized by suppressing the spurious generation of standing waves. However, a nonlinear simulation can be initialized with simple linear waves if the runtime is long enough to adjust the wave shape [*Dommermuth*, 2000]. As can be seen in the bottom panel of Figure 1, the amplitude of the first harmonic remains constant during the propagation while the amplitudes of the higher harmonics tend to increase until a constant value is reached, as illustrated in *Dommermuth* [2000]. For this reason, no adjustment is required in our case.

[14] We generate only a finite number N_w of waves with period $T_0 = 2\pi/\omega$, and thus, the wave generation time T is defined as $T = N_w T_0$. The monochromatic deviation of the free surface at the left boundary is then propagated toward the right wall under the SGN dynamics. The length L of the computational domain and the final simulation time T_f are

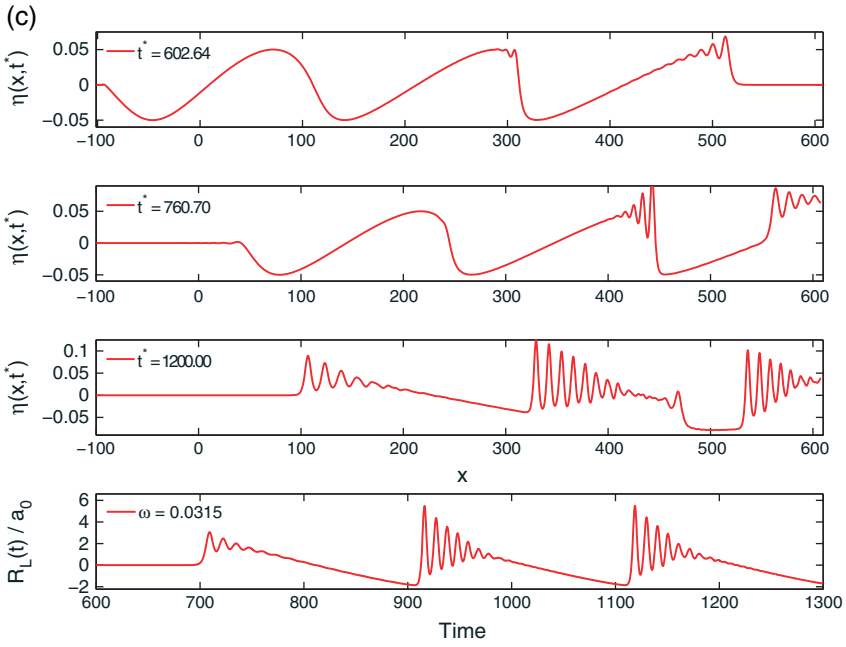

Figure 2. (continued)

chosen adaptively in order to allow all important interactions and to prevent any kind of reflections with the left generating boundary:

$$L = \left(N_w + \frac{1}{2}\right)\lambda, \quad T_f = \frac{L}{\sqrt{g(d+a_0)}} + T, \tag{6}$$

with λ being the wavelength corresponding to the frequency ω.

2.2. Numerical Results

[15] We begin our numerical experiments by considering a single sinusoidal wave interacting with the solid wall. In Figure 2, we show three snapshots of the single-wave evolution at three different times (first three panels on Figures 2a–2c), i.e., before reaching the wall, during the impact, and right after the reflection. The initial sinusoidal wave undergoes steepening during its propagation. The runup on the vertical wall is shown on the bottom panel of Figures 2a. The maximal dimensionless wave elevation $R_{\max} \simeq 0.10245$ on the wall reaches roughly twice the incident wave amplitude $a_0 = 0.05$ (at $t \simeq 70$). This result is in good agreement with previous numerical studies on the solitary waves interactions [*Cooker et al.*, 1997; *Pelinovsky et al.*, 1999; *Chambarel et al.*, 2009] even if the incident shape is not exactly the same. The maximal relative runup $R_{\max}/a_0 \simeq 2.34$ is achieved for $\omega_{\max} = 0.145$. The value of $R_{\max}$ is slowly decreasing for $\omega > \omega_{\max}$.

[16] When two waves are injected into the domain, the dynamics is similar to the single-wave case. However, with two waves, the nonlinear effects become even more apparent (see the bottom panel of Figure 2b).

[17] In a certain range of wave periods ($\omega \in (0.01, 0.05)$), the so-called *dispersive shock waves* are formed [*Wei et al.*, 1995; *Tissier et al.*, 2011]. This particular type of solution has been extensively studied theoretically and numerically in *El et al.* [2006]. When the second wave impinges on the first reflected wave, a dispersive shock wave forms and propagates toward the wall. As shown in the bottom panel of Figure 2b, the maximal amplification is achieved when the second wave hits the wall due to nonlinear interactions between two counter-propagating waves. However, we underline that with only two waves, one can achieve a maximal runup on the wall $R_{\max}$ of almost four incident wave amplitudes a_0: $R_{\max}/a_0 \simeq 3.8$, for $\omega = 0.021$. Such high runup values are possible due to the energy transfer between the first reflected wave and the second incoming wave. The dependence of the maximal runup $R_{\max}$ on the incident wave frequency ω and the number N_w of incident waves is shown in Figure 3. One can see from this figure that the optimal energy transfer due to dispersive shocks happens

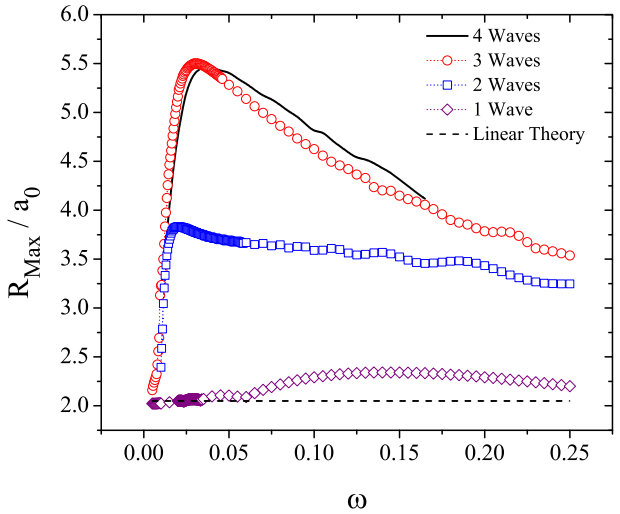

Figure 3. Maximum wave runup $R_{\max}/a_0$ on the right vertical wall as a function of incoming wave frequency for different numbers of incident pulses: 1 (diamonds), 2 (squares), 3 (circles), and 4 (solid line). The dashed line represents the linear limit where $R_{\max}/a_0 \equiv 2$.

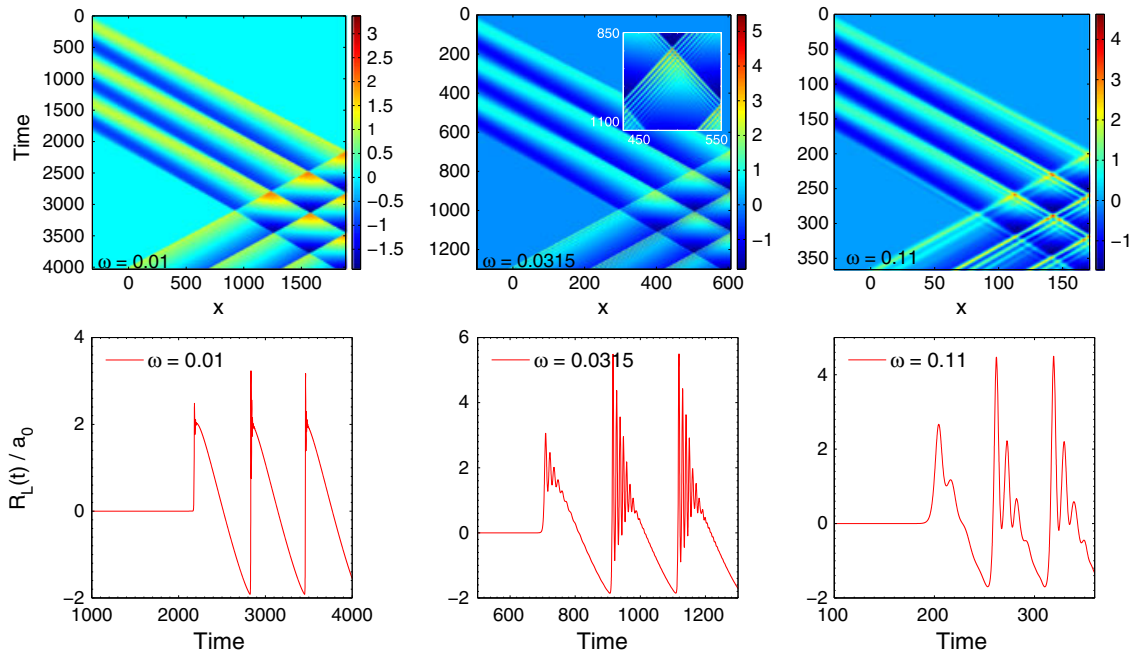

Figure 4. (top) Space-time evolution plots for the three incident wave case shown for three particular values of the wave frequency ω. (bottom) Time evolution of the wave runup on the vertical wall for the three incident wave case recorded for several values of the incoming frequency ω. The maximum runup is achieved for $\omega_{max} \approx 0.0315$.

for three incident waves (see the bottom panel of Figure 2c). In this case, the maximal runup is observed around $\omega_{max} = 0.035$, and the amplification is equal to $R_{max}/a_0 \simeq 5.43$. However, the energy transfer process is saturated for three waves.

[18] We performed similar computations with four incident waves (also shown on Figure 3), and the maximal runup is not higher than with three waves. Consequently, we focus now only on the *optimal* three-wave case. The three regimes (hyperbolic, equilibrium, and dispersive) are illustrated on Figure 4, where we show the space-time dynamics of the three-wave system. The left panel shows the hyperbolic regime. On the central panel, strong dispersive shocks can be observed, while on the right panel, the dynamics is smoothed by the dispersion. In the last case, the amplification is mainly produced by the linear superposition of the incident and reflected waves. The reflection and interaction are clearly observed by smooth secondary peaks in the space-time plots (see Figure 4, bottom panels).

[19] The wave interactions described above strongly depend on the frequency ω of the impinging waves as can be seen in the bottom panels of Figure 4, where we show the wave records on the wall for several values of the frequency ω. As the wave frequency increases, the wavelength shortens and the dispersive effects become gradually more important. Around ω_{max}, the dispersive effects are balanced with nonlinearities to produce the most pronounced dispersive shock waves. Starting from $\omega \simeq 0.11$, we enter into the dispersive regimes where the waves become regularized.

3. Conclusions and Perspectives

[20] In the present study, we investigated numerically the interaction between a wave and a vertical wall in the framework of the Serre-Green-Naghdi (SGN) equations. These equations combine strong nonlinear and weak dispersive effects. We explored the whole range of wavelengths from the hyperbolic regime (including shock waves) to smooth dispersive waves ($\omega \gtrsim 0.1$). More importantly, we showed that the wave runup on the wall is strongly dependent on the incident wave frequency, the dependence not being monotonic. In particular, there is a fixed frequency ω_{max} which provides the maximum long wave runup on the vertical wall. The function $R_{max}(\omega)$ is monotonically increasing up to ω_{max} and monotonically decreasing for $\omega > \omega_{max}$ (at least within the range of considered numerical parameters). The dynamics can be conventionally divided into three main stages: propagation of the wave group toward the wall along with the front steepening and other nonlinear deformations, first wave runup and its reflection from the wall, and projection of the reflected energy again onto the wall by subsequent incident waves. The maximal observed amplification $\approx 5.5a_0$ is achieved with only three incident waves. For example, on a 10 *m* water depth the *critical* period is equal approximatively to $T_{max} \approx 180$ *s* ($\omega_{max} \equiv 2\pi/T_{max}$). Such a wave period can be generated by small underwater landslides.

[21] The results presented in this study shed light onto extreme wave runups on vertical cliffs and similar coastal structures. Moreover, in view of these results, the definition of the *design wave* has to be revisited. Our suggestion would be to take at least $3H_{1/3}$ or even $3H_{1/10}$. The present results also shed some new light on the mysterious accumulations of large boulders on cliff tops up to 50 m high on the deep water coasts, especially on the west coast of Ireland [*Hansom and Hall*, 2009; *Williams*, 2010; *O'Brien et al.*, 2013]. The emplacement of these megaclasts is usually attributed to extreme storm waves, but there are also those who believe that tsunamis are the most probable explanation of boulder ridges in these areas [*Kelletat*, 2008; *Scheffers et al.*, 2009, 2010].

[22] In future investigations, more general wave groups have to be studied to unveil their potential for focusing on the walls. We recall that so far, we considered only simple idealized monochromatic waves. In addition, we are going to investigate the effect of the forces exerted by incident waves on vertical obstacles, which can be different from the purely kinematic amplitude focusing presented in this study. In other words, it is not clear whether the highest wave will produce the highest dynamic pressure spike on the wall. The effect of the wave amplitude is to be investigated as well since all the processes under consideration are highly nonlinear. Some theoretical explanation of these phenomena is also desirable. However, the difficulty is rather high again because of important nonlinearities mentioned hereinabove. We claim that no linear theory is sufficient to provide a satisfactory explanation.

[23] **Acknowledgments.** This work was funded by ERC under the research project ERC-2011-AdG 290562-MULTIWAVE and SFI under grant SFI/12/ERC/E2227. The authors wish to acknowledge the SFI/HEA Irish Centre for High-End Computing (ICHEC) for the provision of computational facilities and support under the project "*Numerical simulation of the extreme wave run-up on vertical barriers in coastal areas*." We would like also to thank Alizée DUBOIS who obtained the first preliminary results on this subject during her visit to University College Dublin in May 2012.

[24] The Editor thanks two anonymous reviewers for their assistance in evaluating this paper.

References

Berger, K. M., and P. A. Milewski (2003), Simulation of wave interactions and turbulence in one-dimensional water waves, *SIAM J. Appl. Math.*, *63*(4), 1121–1140.

Bona, J. L., and M. Chen (1998), A Boussinesq system for two-way propagation of nonlinear dispersive waves, *Physica D*, *116*, 191–224.

Bona, J. L., W. G. Pritchard, and L. R. Scott (1980), Solitary-wave interaction, *Phys. Fluids*, *23*, 438–441.

Byatt-Smith, J. G. B. (1988), The reflection of a solitary wave by a vertical wall, *J. Fluid Mech.*, *197*, 503–521.

Carter, J. D., and R. Cienfuegos (2011), The kinematics and stability of solitary and cnoidal wave solutions of the Serre equations, *Eur. J. Mech. B Fluids*, *30*, 259–268.

Chambarel, J., C. Kharif, and J. Touboul (2009), Head-on collision of two solitary waves and residual falling jet formation, *Nonlinear Processes Geophys.*, *16*, 111–122.

Chazel, F., D. Lannes, and F. Marche (2011), Numerical simulation of strongly nonlinear and dispersive waves using a Green-Naghdi model, *J. Sci. Comput.*, *48*, 105–116.

Clamond, D., and D. Dutykh (2012), Practical use of variational principles for modeling water waves, *Physica D*, *241*(1), 25–36, doi:10.1016/j.physd.2011.09.015.

Clamond, D., M. Francius, J. Grue, and C. Kharif (2006), Long time interaction of envelope solitons and freak wave formations, *Eur. J. Mech. B Fluids*, *25*(5), 536–553, doi:10.1016/j.euromechflu.2006.02.007.

Cooker, M. J., P. D. Weidman, and D. S. Bale (1997), Reflection of a high-amplitude solitary wave at a vertical wall, *J. Fluid Mech.*, *342*, 141–158.

Craig, W., P. Guyenne, J. Hammack, D. Henderson, and C. Sulem (2006), Solitary water wave interactions, *Phys. Fluids*, *18*(5), 57,106, doi:10.1063/1.2205916.

Dias, F., and P. Milewski (2010), On the fully-nonlinear shallow-water generalized Serre equations, *Phys. Lett. A*, *374*(8), 1049–1053.

Dommermuth, D. (2000), The initialization of nonlinear waves using an adjustment scheme, *Wave Motion*, *32*, 307–317.

El, G. A., R. H. J. Grimshaw, and N. F. Smyth (2006), Unsteady undular bores in fully nonlinear shallow-water theory, *Phys. Fluids*, *18*, 27,104.

Fenton, J. D., and M. M. Rienecker (1982), A Fourier method for solving nonlinear water-wave problems: Application to solitary-wave interactions, *J. Fluid Mech.*, *118*, 411–443, doi:10.1017/S0022112082001141.

Goda, Y. (2010), *Random Seas and Design of Maritime Structures, Adv. Ser. on Ocean Eng.*, vol. 33, World Sci., Singapore.

Green, A. E., and P. M. Naghdi (1976), A derivation of equations for wave propagation in water of variable depth, *J. Fluid Mech.*, *78*, 237–246.

Green, A. E., N. Laws, and P. M. Naghdi (1974), On the theory of water waves, *Proc. R. Soc. London, Ser. A*, *338*, 43–55.

Hammack, J., D. Henderson, P. Guyenne, and M. Yi (2004), Solitary wave collisions, *Proceedings of 23rd International Conference on Offshore Mechanics and Arctic Engineering, June 20-25, 2004*, Vancouver, BC, Canada.

Hansom, J., and A. Hall (2009), Magnitude and frequency of extra-tropical North Atlantic cyclones: A chronology from cliff-top storm deposits, *Quat. Int.*, *195*, 42–52.

Kelletat, D. (2008), Comments to Dawson, A. G. and Stewart, I. (2007). Tsunami deposits in the geological record.-Sedimentary Geology 200, 166-183, *Sediment. Geol.*, *211*, 87–91.

Lannes, D., and P. Bonneton (2009), Derivation of asymptotic two-dimensional time-dependent equations for surface water wave propagation, *Phys. Fluids*, *21*, 016601.

Li, Y. A. (2002), Hamiltonian structure and linear stability of solitary waves of the Green-Naghdi equations, *J. Nonlinear Math. Phys.*, *9*(1), 99–105.

Linton, C. M., and P. McIver (2001), *Mathematical Techniques for Wave/Structure Interactions*, 320 pp., Chapman and Hall, Loughborough University, UK.

Maxworthy, T. (1976), Experiments on collisions between solitary waves, *J. Fluid. Mech.*, *76*, 177–185.

Mei, C. C. (1989), *The Applied Dynamics of Ocean Surface Waves*, World Sci., Singapore.

Mirchina, N. R., and E. Pelinovsky (1984), Increase in the amplitude of a long wave near a vertical wall, *Izv. Atmos. Oceanic Phys.*, *20*(3), 252–253.

O'Brien, L., J. M. Dudley, and F. Dias (2013), Extreme wave events in Ireland: 14 680 BP–2012, *Nat. Hazards and Earth Sys. Sci.*, *13*(3), 625–648, http://www.nat-hazards-earth-syst-sci.net/13/625/2013/, doi:10.5194/nhess-13-625-2013.

Pelinovsky, E. N., E. Troshina, V. Golinko, N. Osipenko, and N. Petrukhin (1999), Runup of tsunami waves on a vertical wall in a basin of complex topography, *Phys. Chem. Earth B*, *24*(5), 431–436.

Sainflou, M. (1928), Essai sur les digues maritimes verticales, *Ann. Ponts Chaussées*, *98*(11), 5–48.

Scheffers, A., S. Scheffers, D. Kelletat, and T. Browne (2009), Wave-emplaced coarse debris and megaclasts in Ireland and Scotland: Boulder transport in a high-energy littoral environment, *J. Geol.*, *117*(5), 553–573.

Scheffers, A., D. Kelletat, S. Haslett, S. Scheffers, and T. Browne (2010), Coastal boulder deposits in Galway Bay and the Aran Islands, western Ireland, *Z. Geomorphol.*, *54*(3), 247–279.

Serre, F. (1953), Contribution à l'étude des écoulements permanents et variables dans les canaux, *La Houille Blanche*, *8*, 374–872.

Shampine, L. F. (1994), ODE solvers and the method of lines, *Numer. Methods PDE*, *10*(6), 739–755, doi:10.1002/num.1690100608.

Shampine, L. F., and M. W. Reichelt (1997), The MATLAB ODE Suite, *SIAM J. Sci. Comput.*, *18*, 1–22.

Stoker, J. J. (1957), *Water Waves: The Mathematical Theory With Applications*, Interscience, New York.

Su, C. H., and R. M. Mirie (1980), On head-on collisions between two solitary waves, *J. Fluid Mech.*, *98*, 509–525.

Tissier, M., P. Bonneton, F. Marche, F. Chazel, and D. Lannes (2011), Nearshore dynamics of tsunami-like undular bores using a fully nonlinear Boussinesq model, *J. Coastal Res.*, *64*, 603–607.

Wei, G., J. T. Kirby, S. T. Grilli, and R. Subramanya (1995), A fully nonlinear Boussinesq model for surface waves. Part 1. Highly nonlinear unsteady waves, *J. Fluid Mech.*, *294*, 71–92.

Williams, D. M. (2010), Mechanisms of wave transport of megaclasts on elevated cliff-top platforms: Examples from western Ireland relevant to the storm-wave versus tsunami controversy, *Irish J. Earth Sci.*, *28*, 13–23.

Zabusky, N. J., and M. D. Kruskal (1965), Interaction of "solitons" in a collisionless plasma and the recurrence of initial states, *Phys. Rev. Lett.*, *15*, 240–243.

Zheleznyak, M. I., and E. N. Pelinovsky (1985), *Physical and mathematical models of the tsunami climbing a beach*, in *Tsunami Climbing a Beach*, edited by Pelinovsky, E. N., Appl. Phys. Inst. Press, Gorky.